ISSN (Print) 1226-1750
ISSN (Online) 2233-6656
Journal of Magnetics 19(4), 333-339 (2014) http://dx.doi.org/10.4283/JMAG.2014.19.4.333

Growth of Oriented Thick Films of $BaFe_{12}O_{19}$ by Reactive Diffusion

John G. Fisher*, Hung Vu, and Muhammad Umer Farooq

School of Materials Science and Engineering, Chonnam National University, Gwangju 500-757, Korea

(Received 30 April 2014, Received in final form 29 October 2014, Accepted 31 October 2014)

Single crystal growth of $BaFe_{12}O_{19}$ by the solid state crystal growth method was attempted. Seed crystals of α-Fe_2O_3 were pressed into pellets of $BaFe_{12}O_{19}$ + 2 wt % $BaCO_3$ and heat-treated at temperatures between 1150°C and 1250°C for up to 100 hours. Instead of single crystal growth taking place on the seed crystal, BaO diffused into the seed crystal and reacted with it to form a polycrystalline reaction layer of $BaFe_{12}O_{19}$. The microstructure, chemical composition and structure of the reaction layer were studied using scanning electron microscopy-energy dispersive spectroscopy (SEM-EDS), x-ray Diffraction (XRD) and micro-Raman scattering and confirmed to be that of $BaFe_{12}O_{19}$. XRD showed that the reaction layer shows a strong degree of orientation in the (*h*00)/(*hk*0) planes in the sample sintered at 1200°C. $BaFe_{12}O_{19}$ layers with a degree of orientation in the (*hk*0) planes could also be grown by heat-treating an α-Fe_2O_3 seed crystal buried in $BaCO_3$ powder.

Keywords : $BaFe_{12}O_{19}$, single crystal growth, oriented thick film, microstructure, Raman scattering

1. Introduction

Hexagonal ferrites are a class of ferrite materials based on the magnetoplumbite structure [1]. The base material is $BaFe_{12}O_{19}$, also known as M-type hexagonal ferrite. $BaFe_{12}O_{19}$ has a hexagonal unit cell, with a major preferred axis along the c axis and a high degree of magnetocrystalline anisotropy. By combining different ratios of M-type hexagonal ferrites with spinel ferrites, a family of hexagonal ferrites is created. These hexagonal ferrites include W-type ($BaMe_2Fe_{16}O_{27}$), Y-type ($BaMe_2Fe_{12}O_{22}$), X-type ($Ba_2Me_2Fe_{28}O_{46}$), Z-type ($Ba_3Me_2Fe_{24}O_{41}$) and U-type ($Ba_4Me_2Fe_{36}O_{60}$), where Me is a divalent metal ion [1, 2]. Hexagonal ferrites find applications in microwave devices such as phase shifters and antennas [2-4].

Single crystals of $BaFe_{12}O_{19}$ have applications in circulators, filters and phase shifters due to their high saturation magnetization, high magnetocrystalline anisotropy and low ferromagnetic resonance losses [5]. Single crystals of $BaFe_{12}O_{19}$ are grown by the flux method [6-8] or by top seeded solution growth [9]. The flux method is limited in the size of crystals that can be grown. Top seeded solution growth can grow large crystals but is slow and requires expensive crystal growth furnaces and Pt crucibles. Polycrystalline $BaFe_{12}O_{19}$ ceramics can be produced much more quickly and cheaply, but the random orientation of their grains results in larger ferromagnetic resonance losses [5]. The properties of bulk $BaFe_{12}O_{19}$ ceramics can be improved by preparing ceramics with a high degree of grain orientation [5, 10, 11]. Oriented thick films can also be prepared by liquid phase epitaxy [12, 13].

An alternative method of growing single crystals is that of Solid State Crystal Growth (SSCG) [14]. In the SSCG method, a piece of single crystal, called the seed crystal, is buried in ceramic powder of the desired crystal composition and the seed and powder then pressed to form a pellet. This pellet is then sintered and a single crystal of the powder composition grows on the seed crystal. This technique has the advantage of using conventional furnaces and ceramic processing equipment. SSCG has been used to grow single crystals of $BaTiO_3$ [15], Mn-Zn ferrite [16], PMN-PT [17] and $(K_{0.5}Na_{0.5})NbO_3$ [18]. For this technique to work, the seed crystal must have the following properties: it should have the same structure as the single crystal, it should have similar unit cell parameters and it should be chemically compatible with the ceramic matrix [14, 19]. In this regard, α-Fe_2O_3 (hematite) may be a suitable material for the seed crystal. α-Fe_2O_3 and $BaFe_{12}O_{19}$ both have hexagonal unit cells, with space groups *P63/mmc* and *R-3c* for $BaFe_{12}O_{19}$ and α-Fe_2O_3 respectively [20]. The unit cell parameters for $BaFe_{12}O_{19}$ are a = 0.5893 nm and c = 2.3194 nm, whereas the unit cell parameters

©The Korean Magnetics Society. All rights reserved.
*Corresponding author: Tel: +82-62-530-1702
Fax: +82-62-530-1699, e-mail: johnfisher@jnu.ac.kr

© 2014 Journal of Magnetics

for α-Fe_2O_3 are $a = 0.5112$ nm and $c = 1.3382$ nm [20]. In addition, $BaFe_{12}O_{19}$ and α-Fe_2O_3 form a two-phase field in the BaO-Fe_2O_3 phase diagram, indicating their chemical compatibility [21]. In the present work, we describe attempts to grow single crystals of $BaFe_{12}O_{19}$ by SSCG using α-Fe_2O_3 as the seed crystal.

2. Experimental

A commercial M-type barium hexaferrite $BaFe_{12}O_{19}$ powder (99.2%, supplied by LG Innotek Co. Ltd., LG Components R&D Center) was used. 2 wt % of $BaCO_3$ (Alfa Aesar 99.8%) was added to the powder to promote single crystal growth. Mixing was carried out by ball milling in ethanol with stainless steel media in a polypropylene jar for 24 hours. After evaporating the ethanol with a hot plate and stirrer, the powder was ground in an agate mortar and pestle and sieved to pass a 180 μm mesh sieve.

Single crystals of α-Fe_2O_3 (naturally occurring) were used as seed crystals. Seed crystals of size 2 × 2 × 0.5-0.7 mm, cut approximately parallel to the basal plane, were cut from the α-Fe_2O_3 single crystal using a low speed diamond wheel saw. One side of each seed crystal was polished to a 1 μm finish with SiC papers and diamond suspension. To prepare a sample, a seed crystal was buried in 0.7 g of powder in a steel die of 10 mm diameter. The powder is hand pressed, and the pellet is removed from the die. The pellet is then cold isostatically pressed (CIP) at 1500 kg/cm^2 (147 MPa) pressure. Samples were sintered in the temperature range 1150°C-1250°C for 20 or 100 hours with heating and cooling rates of 2°C/min. To reduce Ba volatilization, samples were buried in $BaFe_{12}O_{19}$ (Kojundo, 99%) packing powder in a double alumina crucible with lids. Samples were vertically sectioned using a low speed diamond wheel saw, polished to a 1 μm finish and thermally etched. Some samples were also polished horizontally i.e. in the plane of the seed and single crystal. The microstructure of the samples was analyzed using scanning electron microscopy (SEM, Hitachi S-4700 FESEM, Hitachi High-Tech, Tokyo, Japan) with an attached energy dispersive spectrometer with standardless quantification (EDS, EMAX Energy EX-200, Horiba, Kyoto, Japan).

For x-ray diffraction (XRD, D/MAX Ultima III, Rigaku, Tokyo, Japan), one of the samples that had been sintered at 1200°C for 100 hours was vertically sectioned and polished. It was then polished in the horizontal plane of the seed crystal to a 1 μm finish. By careful polishing, it was possible to remove the ceramic matrix from the top face of the sample, thereby exposing the grown single crystal on one face. At this point, the ceramic matrix still surrounds the sides of the single crystal. XRD was carried out using Cu Kα radiation, a scan range of 20-90° of 2θ, a step size of 0.013° and a scan speed of 1°/min. The surrounding ceramic matrix was then cut away using a low speed diamond saw and XRD was repeated.

For micro-Raman analysis, a LabRam HR800 UV (Horiba Jobin-Yvon, France) Raman microscope with 514 nm diode laser and 10 mW power was used at room temperature. A vertically sectioned and polished sample sintered at 1200°C for 20 hours was examined. This sample was not thermally etched. Spectra were taken on the α-Fe_2O_3 seed crystal, the single crystal and the surrounding ceramic matrix. The spectra were collected in backscattered geometry, with a resolution of ~0.3 cm^{-1} and a charge coupled device detector. The diameter of the laser spot on the sample is 1-2 μm.

3. Results

SEM micrographs of the sample sintered for 20 hours are shown in Fig. 1. In the samples sintered at 1150°C and 1200°C, a single crystalline reaction layer of $BaFe_{12}O_{19}$ appears to have grown on the Fe_2O_3 seed crystal [Fig. 1(a) and (b)]. For the sample sintered at 1250°C, a $BaFe_{12}O_{19}$ polycrystalline layer has grown on the seed crystal [Fig. 1(c)]. From measurements of the seed crystal thickness before and after the crystal growth experiments, it is seen that the $BaFe_{12}O_{19}$ reaction layers have grown *into* the seed crystal, rather than out into the polycrystalline matrix. The $BaFe_{12}O_{19}$ reaction layer grows on both sides of the seed crystal; polishing one face of the seed crystal does not affect the growth distance of the reaction layer. The orientation of the reaction layer at the edges of the seed crystal differs from that of the reaction layer along the plane faces of the seed crystal (not shown here). The thickness of the reaction layer increases with sintering temperature and time. By sintering at 1200°C for 100 hours, a reaction layer ~260 μm thick could be grown. The interface between the reaction layer and the seed crystal becomes irregular with increasing sintering temperature, as does the interface between the reaction layer and the polycrystalline matrix. The matrix grain size of the sample sintered at 1150°C for 20 hours varies between 0.5-2 μm. Abnormal grain growth takes place in the samples sintered at 1200°C and 1250°C for 20 hours, with grains up to 100 μm in diameter.

The reaction layer of the sample sintered at 1200°C for 20 hours is shown at higher magnification in Fig. 2. The reaction layer is not truly single crystalline but consists of oriented columnar grains [Fig. 2(a)]. The orientation of the grains appears to decrease at the interface of the reac-

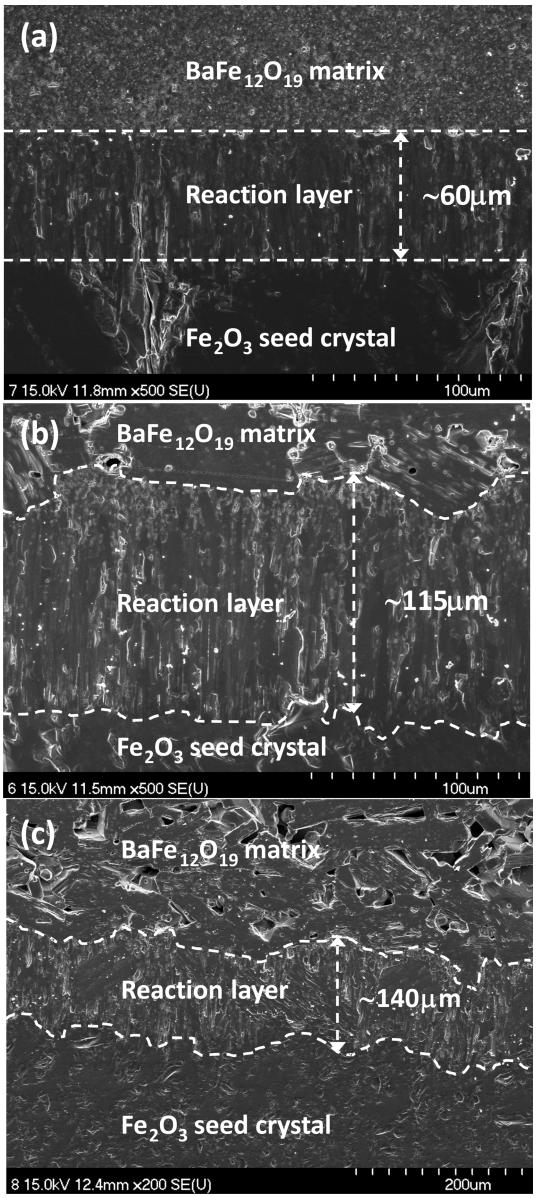

Fig. 1. SEM micrographs of samples sintered for 20 hours at (a) 1150°C, (b) 1200°C and (c) 1250°C.

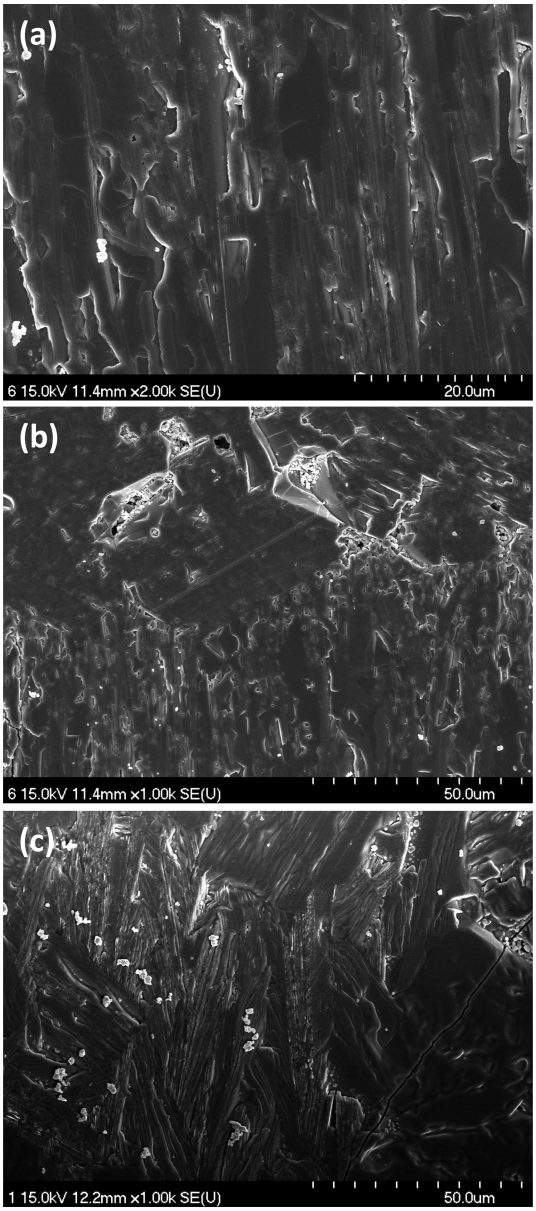

Fig. 2. SEM micrographs of (a) the reaction layer and (b) the reaction layer/polycrystalline matrix interface of the sample sintered at 1200°C for 20 hours. Fig. 2(c) shows the horizontal plane of the reaction layer of a sample sintered at 1200°C for 100 hours.

tion layer and the polycrystalline matrix [Fig. 2(b)]. A micrograph taken in the horizontal plane of the reaction layer of a sample sintered at 1200°C for 100 hours is shown in Fig. 2(c). This sample was also polished and etched. The micrograph shows grains arranged both perpendicular and parallel to the horizontal plane of the sample. The vertically aligned grains are growing in various directions i.e. there is little alignment of the grains in the horizontal plane of the sample. EDS of the white particles in Fig. 2(c) show them to contain Si and Zr as well as Ba, Fe and O. These may be caused by impurities present in the seed crystal. EDS results for a sample sintered at 1200°C for 100 hours are shown in Table 1 (this sample was polished but not etched). The analysis results for the reaction layer and the matrix are each the mean and standard deviation of five analysis points. Both the reaction layer and the matrix grains have a chemical composition close to the nominal composition for $BaFe_{12}O_{19}$.

XRD traces of the sintered sintered at 1200°C for 100 hours are shown in Fig. 3. Both traces can be indexed with ICDD pattern #84-0757 for $BaFe_{12}O_{19}$. For clarity, only the (h00)/(hk0) peaks are labelled. The lower pattern is from the reaction layer and the surrounding matrix. In

Table 1. EDS analysis of the sample sintered at 1200°C for 100 hours.

	Reaction layer	Matrix	$BaFe_{12}O_{19}$ nominal
Ba	3.5 ± 0.1	3.7 ± 0.2	3.1
Fe	40.5 ± 0.8	40.8 ± 2.2	37.5
O	55.9 ± 0.9	55.4 ± 2.3	59.4

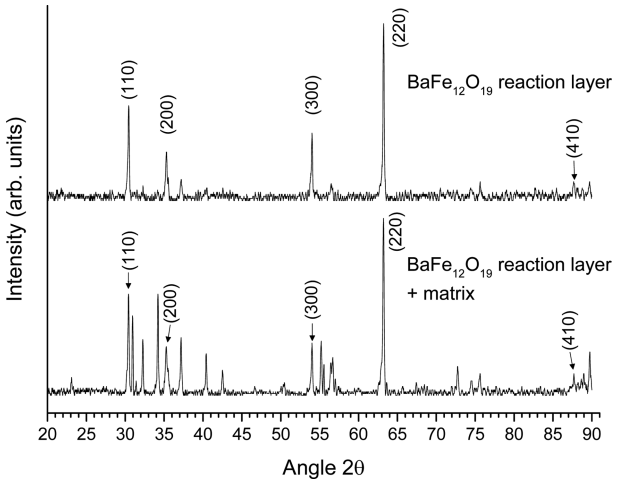

Fig. 3. XRD traces of the horizontal plane of the sample sintered at 1200°C for 100 hours.

this sample, strong (110) and (220) peaks can be seen, showing a preferred orientation. The upper pattern shows the sample after most of the surrounding ceramic matrix has been cut away. Strong (110), (220), (200) and (300) peaks can be seen. This shows that the reaction layer has a strong (*h*00)/(*hk*0) orientation. The other peaks in this trace may come from matrix grains that could not be removed, from grains in the reaction layer which are not oriented or from the edges of the reaction layer where the orientation is different to that of the plane faces.

Micro-Raman spectra of the sample sintered at 1200°C for 20 hours are shown in Fig. 4. The spectrum for the seed crystal contains seven main peaks. These peak positions lie close to or on the positions for hematite (α-Fe_2O_3) [22]. The spectra for the reaction layer and the polycrystalline matrix are similar to each other. Both spectra contain peaks associated with $BaFe_{12}O_{19}$ [23-25]. There are some differences in peak position and intensity between the reaction layer and the polycrystalline matrix. The differences in peak position may be caused by strains in the reaction layer [26]. The polycrystalline matrix has a peak at 461 cm^{-1} which is absent in the reaction layer. Differences in peak intensity between the reaction layer and the polycrystalline matrix may be due to differences in composition [25] or crystallographic orientation [26].

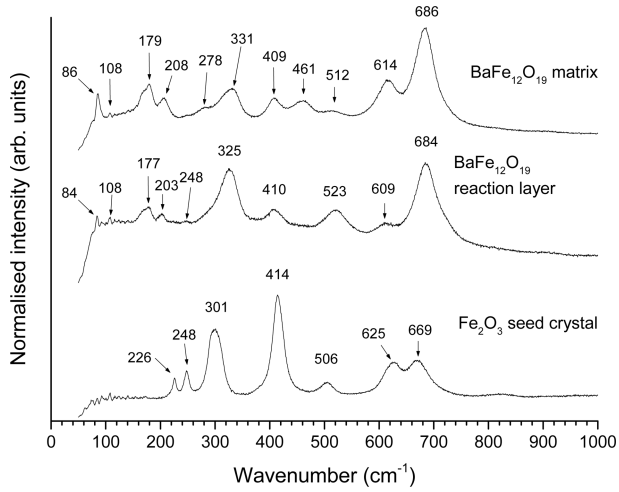

Fig. 4. Micro-Raman spectra of the sample sintered at 1200°C for 20 hours.

4. Discussion

Contrary to our expectations, crystal growth of $BaFe_{12}O_{19}$ by solid state crystal growth did not take place. Little matrix grain growth took place in the sample sintered at 1150°C, indicating that the sintering temperature may have been too low to promote single crystal growth on the seed crystal. In the samples sintered at 1200°C and 1250°C, abnormal grain growth in the matrix would have rapidly reduced the driving force for single crystal growth on the seed crystal, again preventing single crystal growth [27].

Excess $BaCO_3$ was added to the $BaFe_{12}O_{19}$ powder to promote single crystal growth as it is known to promote abnormal grain growth [28], which is a prerequisite for solid state crystal growth [19]. However, the $BaCO_3$ appears to have reacted directly with the α-Fe_2O_3 seed crystal to form $BaFe_{12}O_{19}$. According to the work of Wang *et al.*, the formation of $BaFe_{12}O_{19}$ from $BaCO_3$ and α-Fe_2O_3 takes place by a two-step reaction [29]. $BaCO_3$ first reacts with α-Fe_2O_3 at ~700°C to form $BaFe_2O_4$ according to the reaction:

$$BaCO_3 + Fe_2O_3 \rightarrow BaFe_2O_4 + \uparrow CO_2 \quad (1)$$

The $BaFe_2O_4$ then reacts with α-Fe_2O_3 at temperatures higher than 770°C to form $BaFe_{12}O_{19}$ via the reaction:

$$BaFe_2O_4 + 5Fe_2O_3 \rightarrow BaFe_{12}O_{19} \quad (2)$$

Similar results were also found earlier by Steier *et al.*, who also used transmission electron microscopy to study the reaction between $BaCO_3$ and α-Fe_2O_3 [30]. They found that after the formation of a $BaFe_{12}O_{19}$ monolayer at the $BaFe_2O_4$/α-Fe_2O_3 interface, Ba^{2+} ions diffuse through

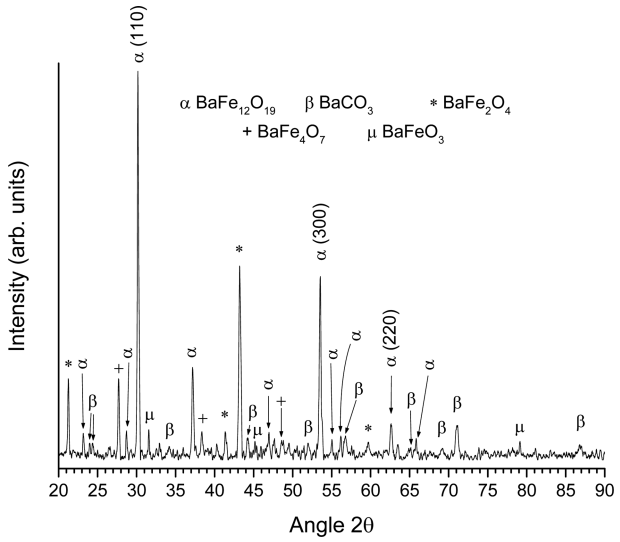

Fig. 5. XRD trace of an α-Fe_2O_3 seed crystal heat treated in $BaCO_3$ at 1200°C for 20 hours.

the $BaFe_{12}O_{19}$ crystal lattice and the $BaFe_{12}O_{19}$ phase grows into the α-Fe_2O_3 phase. We believe that growth of the $BaFe_{12}O_{19}$ reaction layer in the present work takes place via the same mechanism. Additionally, Ba^{2+} ions can diffuse along the grain boundaries in the $BaFe_{12}O_{19}$ reaction layer to reach the $BaFe_{12}O_{19}$/α-Fe_2O_3 interface. The results in the present work are similar to the work of Pankov *et al.*, who produced thin films of $BaFe_{12}O_{19}$ by reactive diffusion of $BaFe_2O_4$ thin films deposited on single crystals of α-Fe_2O_3 [31]. The $BaFe_{12}O_{19}$ thin film grown by Pankov *et al.* had a (00*l*) preferred orientation, whereas the thick films prepared in the present work have a (*h*00)/(*hk*0) orientation. The reason for this difference is not known. Also, the role that the $BaFe_{12}O_{19}$ matrix grains play in the growth of the reaction layer in the present work needs further investigation.

To check if a reaction layer could be grown in the absence of $BaFe_{12}O_{19}$ matrix grains, a seed crystal of α-Fe_2O_3 was buried in $BaCO_3$ powder in an alumina crucible with lid and heat-treated at 1200°C for 20 hours. An XRD trace of the face of the seed crystal is shown in Fig. 5. The α-Fe_2O_3 seed crystal has reacted with the $BaCO_3$ to form $BaFe_{12}O_{19}$ (ICDD card # 78-0133, hexagonal, space group *P63/mmc*), which appears to show a degree of orientation in the (*hk*0) planes. Unreacted $BaCO_3$ is present (ICDD card #s 85-0720 and 74-1626), along with secondary phases of $BaFe_2O_4$ (ICDD card # 70-1441), $BaFe_4O_7$ (ICDD card # 70-1299) and $BaFeO_3$ (ICDD card # 85-0852). An SEM micrograph of the polished cross-section of the sample is shown in Fig. 6. A double layer approximately 25 μm in thickness has grown on the α-Fe_2O_3 seed crystal. EDS analysis shows that the upper layer has a chemical composition approximately equal to $BaFe_2O_4$ and that the lower layer has a chemical composition approximately equal to $BaFe_{12}O_{19}$. The $BaFe_{12}O_{19}$ layer shows some preferential orientation of the grains.

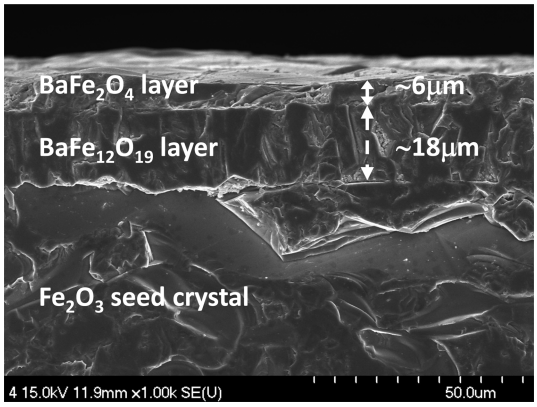

Fig. 6. SEM micrograph of an α-Fe_2O_3 seed crystal heat treated in $BaCO_3$ at 1200°C for 20 hours.

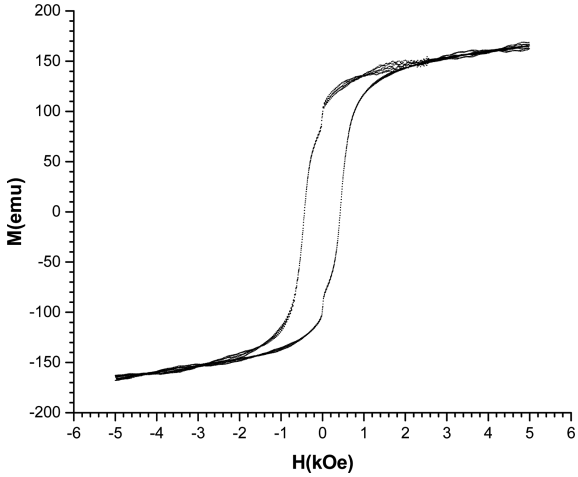

Fig. 7. Magnetic hysteresis loop of an α-Fe_2O_3 seed crystal heat treated in $BaCO_3$ at 1200°C for 20 hours. The magnetic field was applied parallel to the sample surface.

Fig. 7 shows a magnetic hysteresis loop of the sample measured on an Alternating Gradient Magnetometer (Model no. 2900-02 AGM, Princeton Measurements Corporation, Westerville OH, USA). The hysteresis loop is similar in appearance to those of $BaFe_{12}O_{19}$ thin films produced by pulsed laser deposition [32, 33]. The steepness of the M-H curve indicates that the easy axis of magnetization of the reaction layer is partially aligned parallel to the surface of the sample, which agrees with the XRD results in Fig. 5. This is unlike the thin films in refs. [32] and [33], which have their easy axis of magnetization aligned perpendicular to the sample surface. The remanent magnetization M_r is 97 emu and the coercivity H_C is 432 Oe.

With further optimization of the processing parameters

such as heat-treatment temperature and time, this method of direct reaction between the α-Fe_2O_3 seed crystal and $BaCO_3$ powder could provide an alternative and simple way of growing oriented thick films of $BaFe_{12}O_{19}$. Furthermore, the sequence of reactions which take place on the α-Fe_2O_3 seed crystal needs to be studied. For example, the question of whether $BaFe_2O_4$ forms first and then reacts with Fe_2O_3 to form the $BaFe_{12}O_{19}$ reaction layer (as in refs. [29] and [30]), or whether a $BaFe_{12}O_{19}$ reaction layer forms first and then further reacts with the $BaCO_3$ to form $BaFe_2O_4$ and other secondary phases, should be answered. This will be helpful for the growth of oriented $BaFe_{12}O_{19}$ thick films without any secondary phases.

5. Conclusion

Experiments were carried out to grow single crystals of $BaFe_{12}O_{19}$ by solid state crystal growth. Seed crystals of α-Fe_2O_3 were sintered in a matrix of $BaFe_{12}O_{19}$ + 2 wt % $BaCO_3$ at temperatures between 1150°C and 1250°C. Single crystal growth did not take place on the seed crystal. Instead, BaO diffused into the seed crystal and reacted with it to form a polycrystalline reaction layer of $BaFe_{12}O_{19}$. SEM-EDS, XRD and micro-Raman scattering confirmed the chemical composition and structure of the reaction layer as that of $BaFe_{12}O_{19}$. The reaction layer shows a strong degree of orientation in the (*h*00)/(*hk*0) planes in the sample sintered at 1200C. $BaFe_{12}O_{19}$ layers with a degree of orientation in the (*hk*0) planes could also be grown by heat-treating an α-Fe_2O_3 seed crystal in $BaCO_3$ powder.

Acknowledgement

This work was funded by the National Research Foundation of Korea (project no. 2012R1A1A2000925). The authors would like to thank Dr. Won-Ha Moon and Dr. Seok Bae (LG Innotek) for providing the $BaFe_{12}O_{19}$ powder, and Prof. Jong-Sook Lee for providing the α-Fe_2O_3 single crystal. The authors would like to thank Dr. Sang-Hun Jeong (Korea Basic Science Institute, Gwangju center) for carrying out the micro-Raman scattering experiments, and Jeong-Eun Kim and Hye-Jeong Kim for operating the XRD and SEM respectively. The authors would like to thank Prof. Byong-Guk Park (Korea Advanced Institute of Science and Technology) for measuring the magnetic hysteresis loop.

References

[1] A. Goldman, Modern Ferrite Technology 2nd Edition, Springer, New York (2010) pp. 51-70.
[2] J. Jalli, Y. K. Hong, J. J. Lee, G. S. Abo, T. Mewes, B. C. Choi, and S. G. Kim, IEEE Magn. Lett. **2**, 5000104 (2011).
[3] J. Lee, Y. K. Hong, J. Park, W. M. Song, G. H. Kim, and A. Morisako, IEEE Magn. Lett. **2**, 5000204 (2011).
[4] J. Jalli, Y. K. Hong, S. Bae, J. J. Lee, G. S. Abo, J. H. Park, B. C. Choi, T. Mewes, S. G. Kim, S. H. Gee, I. T. Nam, and T. Tanaka, J. Appl. Phys. **109**, 07A509 (2011).
[5] Y. Chen, A. L. Geiler, T. Chen, T. Sakai, C. Vittoria, and V. G. Harris, J. Appl. Phys. **101,** 09M501 (2007).
[6] R. J. Gambino and F. Leonhard, J. Am. Ceram. Soc. **44**, 221 (1961).
[7] J. Jalli, Y. K. Hong, G. S. Abo, S. Bae, J. J. Lee, J. H. Park, B. C. Choi, and S. G. Kim, J. Magn. Magn. Mater. **323**, 2627 (2011).
[8] X. B. Chen, N. T. M. Hien, K. Han, J. Sur, N. H. Sung, B. K. Cho, and I. S. Yang, J. Appl. Phys. **114**, 013912 (2013).
[9] C. Dubs, J. Kräußlich, and P. Görnert, J. Cryst. Growth **318**, 800 (2011).
[10] D. B. Hovis and K. T. Faber, Scripta Mater. **44**, 2525 (2001).
[11] Y. Chen, T. Fitchorov, J. Gao, A. Koblischka-Veneva, M. R. Koblischka, C. Vittoria, and V. G. Harris, Nanotechnology **20**, 445606 (2009).
[12] S. D. Yoon and C. Vittoria, IEEE Trans. Magn. **39**, 3163 (2003).
[13] Y. A. Kranov, A. Abuzir, T. Prakash, D. N. McIlroy, and W. J. Yeh, IEEE Trans. Magn. **42**, 3338 (2006).
[14] H. Y. Lee, Solid-State Single Crystal Growth (SSCG) Method: A Cost-effective Way of Growing Piezoelectric Single Crystals. In: S. Trolier-McKinstry, L. E. Cross and Y. Yamashita (Eds.), Piezoelectric Single Crystals and their Applications, Pennsylvania State University, State College, PA (2003) pp. 160-177.
[15] T. Yamamoto and T. Sakuma, J. Am. Ceram. Soc. **77**, 1107 (1994).
[16] K. Kugimiya, K. Hirota, and K. Matsuyama, Process for Producing Single Crystal Ceramics. US Pat. No. 4900393 (1990).
[17] A. Khan, F. A. Meschke, T. Li, A. M. Scotch, H. M. Chan, and M. P. Harmer, J. Am. Ceram. Soc. **82**, 2958 (1999).
[18] J. G. Fisher, A. Benčan, J. Holc, M. Kosec, S. Vernay, and D. Rytz, J. Crys. Growth **303**, 487 (2007).
[19] A. Benčan, E. Tchernychova, H. Uršič, M. Kosec, and J. G. Fisher, Growth and characterization of potassium sodium niobate single crystals by solid state crystal growth. In: M. Lallart (Ed.), Ferroelectrics-Material aspects, Intech, Croatia (2011) pp. 87-108.
[20] ICDD cards #74-1121 and #88-2359
[21] Y. Goto and T. Takada, J. Am. Ceram. Soc. **43**, 150 (1960).
[22] A. M. Jubb and H. C. Allen, ACS Appl. Mater. Interfaces **2**, 2804 (2010).
[23] J. Kreisel, G. Lucazeau, and H. Vincent, J. Sol. Stat. Chem. **137**, 127 (1998).
[24] J. Kreisel, G. Lucazeau, and H. Vincent, J. Raman Spec-

trosc. **30**, 115 (1999).
[25] W. Y. Zhao, P. Wei, X. Y. Wu, W. Wang, and Q. J. Zhang, J. Appl. Phys. **103**, 063902 (2008).
[26] J. Kreisel, S. Pignard, H. Vincent, J. P. Sénateur, and G. Lucazeau, Appl. Phys. Lett. **73**, 1194 (1998).
[27] J. G. Fisher, A. Benčan, J. Godnjavec, and M. Kosec, J. Eur. Ceram. Soc. **28**, 1657 (2008).
[28] D. B. Hovis, K. T. Faber, and E. A. Kenik, J. Mater. Sci. **43**, 1836 (2008).
[29] H. Z. Wang, Q. He, G. H. Wen, F. Wang, Z. H. Ding, and B. Yao, J. Alloys Compd. **504**, 70 (2010).
[30] H. P. Steir, J. Requena, and J. S. Moya, J. Mater. Res. **14**, 3647 (1999).
[31] V. Pankov, Å. Bartholdson, O. Stukalov, S. Smolenchuk, O. Babushkin, and V. Gremenok, J. Cryst. Growth **252**, 382 (2003).
[32] S. R. Shinde, R. Ramesh, S. E. Lofland, S. M. Bhagat, S. B. Ogale, R. P. sharma, and T. Venkatesan, Appl. Phys. Lett. **72**, 3443 (1998).
[33] Z. Chen, A. Yang, Z. Cai, S. D. Yoon, K. Ziemer, C. Vittoria, and V. G. Harris, IEEE Trans. Magn. **42**, 2855 (2006).